RSC Applied Interfaces

ROYAL SOCIETY OF CHEMISTRY

PAPER

View Article Online
View Journal | View Issue

Cite this: *RSC Appl. Interfaces*, 2026, 3, 84

Plasmon-mediated functionalization of colloidal gold nanoparticles through reductive grafting of diazonium salts under pulsed laser irradiation

Bryan Gosselin,[ab] Maurice Retout, [a] Victor Lepeintre, [ab] Jérôme Tisaun, [c] Claire Mangeney, [d] Cécile Moucheron, [c] Gilles Bruylants *[a] and Ivan Jabin *[b]

Received 15th July 2025,
Accepted 10th November 2025

DOI: 10.1039/d5lf00197h

rsc.li/RSCApplInter

This study introduces an innovative plasmon-mediated strategy for the surface functionalization of colloidal gold nanoparticles (AuNPs) through the reductive grafting of calix[4]arene-based tetra-diazonium salts under pulsed laser irradiation. By exploiting the localized surface plasmon resonance (LSPR) of AuNPs, the diazonium salts were efficiently grafted onto the nanoparticle surface without the use of external reducing agents or photocatalysts. Optimization of experimental parameters, such as irradiation wavelength, power, and reaction time, enabled rapid and robust functionalization while minimizing nanoparticle degradation. Mechanistic studies confirmed that both hot electron generation and localized photothermal effects contribute to the grafting process, while surface analyses confirmed a denser calix[4]arene coating for the particles obtained by photografting. The method was successfully extended to other diazonium salts, with calix[4]arene derivatives yielding densely packed, highly stable organic shells. Compared to conventional chemical reduction, this laser-assisted approach significantly reduces reaction time and reagent consumption. Overall, the method provides a fast, efficient, and versatile strategy for the covalent functionalization of plasmonic nanoparticles in suspension.

Introduction

Plasmonic noble metal nanoparticles (NPs) exhibit remarkable optical properties due to the localized surface plasmon resonance (LSPR) phenomenon.[1] As a result, plasmonic NPs, particularly gold nanoparticles (AuNPs), have found numerous applications in the biomedical field, including *in vitro* diagnostic, drug delivery, and phototherapy.[2–5] In organic synthesis, the photocatalytic activity of plasmonic NPs is particularly valuable for enhancing reaction yields.[6,7] Upon photoexcitation, NPs can act as heat generators or electron reservoirs, enabling the catalysis of various chemical reactions such as dihydrogen dissociation and CO oxidation.[8–10] In 2018, the ability of polyvinylpyrrolidone (PVP) coated-AuNPs to generate "hot electrons" under continuous laser irradiation was evidenced by the reduction of Fe^{3+} complexes.[11] Beyond their applications, the optical properties of NPs can also be exploited for their synthesis or reshaping.[12] For instance, laser-induced synthesis of AuNPs from $AuCl_4^-$ salts and laser-assisted reduction of particle dispersity have been reported.[13]

Functionalization of plasmonic NPs by organic ligands is often essential for ensuring their colloidal stability or tailoring their properties for specific applications. In the case of AuNPs, commonly used ligands include carboxylates, amines, phosphine derivatives and the widely used thiol derivatives.[14,15] Although thiol-based ligands strongly links with or to gold, the S–Au bond remains labile, making them susceptible to detachment in the presence of competing thiols or under thermal conditions.[16,17] An alternative strategy for AuNPs functionalization involves aryl diazonium salts.[18] Upon reduction, these salts generate the corresponding aryl radical species that form strong and irreversible Au–C bonds with gold surfaces.[19] In this context, tetra-diazonium salts based on a calix[4]arene platform have been shown to be particularly effective for the functionalization of AuNPs and AgNPs, yielding ultra-stable and bio-conjugable monolayers.[20–22] Moreover, by adjusting the ratio of two distinct calixarene tetra-diazonium salts, the composition of mixed layers can be controlled.[23,24] Over the past five years, ultra-stable calixarene-based AuNPs and

[a] *Engineering of Molecular NanoSystems, Ecole Polytechnique de Bruxelles, Université libre de Bruxelles (ULB), Avenue F. D. Roosevelt 50, CP165/64, 1050 Brussels, Belgium. E-mail: Ivan.Jabin@ulb.be*
[b] *Laboratoire de Chimie Organique, Faculté des Sciences, Université libre de Bruxelles (ULB), Avenue F. D. Roosevelt 50, CP160/06, 1050 Brussels, Belgium. E-mail: Gilles.Bruylants@ulb.be*
[c] *Laboratoire de Chimie Organique et Photochimie, Faculté des Sciences, Université libre de Bruxelles (ULB), Avenue F. D. Roosevelt 50, CP160/08, 1050 Brussels, Belgium*
[d] *Laboratoire de Chimie et de Biochimie Pharmacologiques et Toxicologiques, CNRS, Université Paris Cité, F-75006 Paris, France*

AgNPs have been applied to the colorimetric detection of biomolecules in solution or in lateral flow assays, delivery of nucleic acids in cells, the immunolabelling of cancer, photothermal therapy, the recovery of precious metals, and oxygen reduction reaction electrocatalysis.[8,25–29]

Despite extensive research on plasmonic NPs, the use of their photocatalytic activity as a tool for their surface functionalization has been scarcely investigated with few examples using iodonium salts or aryl diazonium salts as grafting agents.[30,31] While the photochemical grafting of classical diazonium salts on surfaces has been reported, it usually required the use of a Ru photocatalyst to supply the electrons necessary for reduction.[32] The direct grafting of diazonium salts by UV irradiation has however been demonstrated on metallic surfaces.[33] The grafting of aryl films derived from diazonium salts on gold lithographic nanostripes has been described upon plasmon excitation.[34] This approach enables regioselective functionalization of (an) isotropic structures such as nanodiscs, nanorods or nanotriangles.[35,36] However, these studies have focused exclusively on nanostructures deposited on solid substrates (*e.g.* indium tin oxyde, glass) or lithographed patterns, limiting their potential applications, particularly in *in vivo* drug delivery or phototherapy. To the best of our knowledge, no studies have explored this approach, combining diazonium salt chemistry with plasmon excitation, for NPs in suspension, likely because the functionalization of colloidal NPs requires additional precautions to maintain their stability during the process. Plasmon-induced functionalization of colloidal nanoparticles with diazonium salts could offer several advantages over conventional chemical reduction methods. Notably, this approach may require lower amounts of diazonium salts, as the reduction occurs in close proximity to the NP surface, thereby minimizing uncontrolled polymerization of aryl radicals in solution.[37] Additionally, plasmon-driven functionalization could enable faster and/or regioselective modification of NPs, a benefit previously demonstrated for surface-deposited NPs.[35]

Herein, we present the development of an innovative plasmon-mediated procedure for the efficient functionalization of colloidal gold nanospheres with calix[4] arene tetra-diazonium salts.

Results and discussion

Development of the plasmon-mediated functionalization procedure using calix[4]arene tetra-diazonium salt $X_4(PEG)_4(N_2^+)_4$

To assess the feasibility of the plasmon-mediated functionalization approach, we used a known calix[4]arene tetra-diazonium salt[38] bearing four oligoethylene chains on the small rim, namely $X_4(PEG)_4(N_2^+)_4$ (Fig. 1A). Pulsed laser irradiation of 17 nm AuNPs-citrate was performed in presence of $X_4(PEG)_4(N_2^+)_4$ at 520 nm, corresponding to the LSPR maximum wavelength (LSPR λ_{max}). Note that diazonium

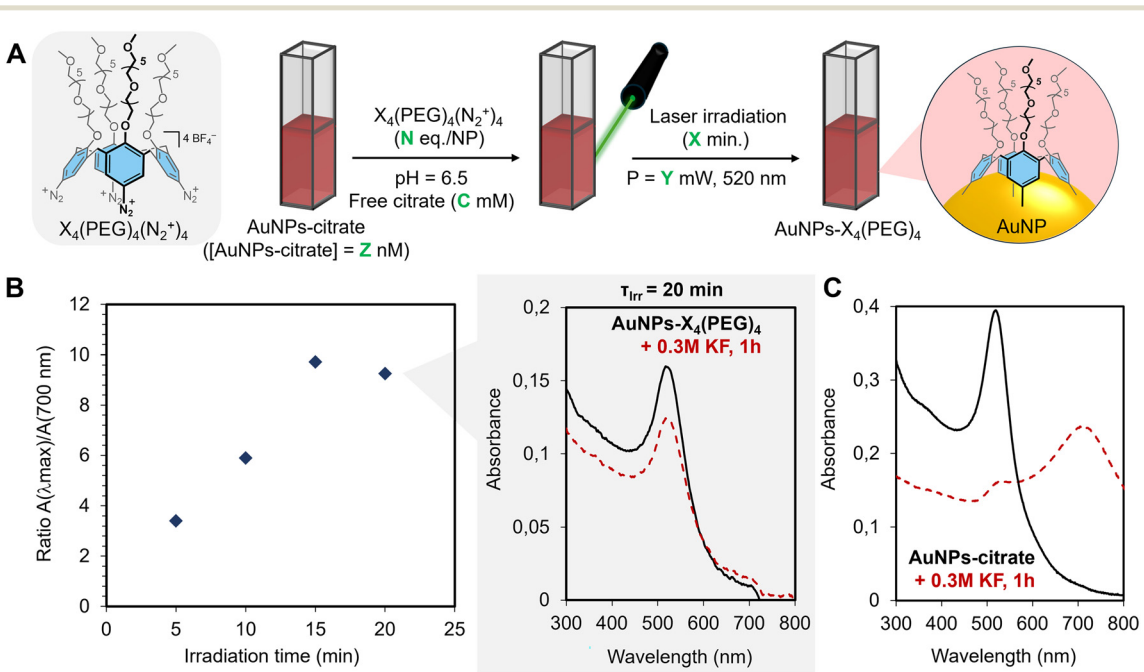

Fig. 1 (A) Photo-mediated grafting of $X_4(PEG)_4(N_2^+)_4$ on AuNPs-citrate. The parameters that have been optimized (N, C, Z, X and Y) are indicated in green. (B) Left: Absorbance ratios ($\lambda_{max}/\lambda_{700\ nm}$) of AuNPs–$X_4(PEG)_4$ after 60 min in the presence of KF as a function of irradiation time. Right: UV-vis spectra in water of AuNPs–$X_4(PEG)_4$ functionalized under 20 minutes of irradiation, before KF addition (black line) and after 60 min in 0.3 M KF (red dashed line). Experimental details: citrate–AuNPs (6 nM) in presence of 0.6 mM citrate; 70 000 eq. of $X_4(PEG)_4(N_2^+)_4$/AuNP; τ_{irr} = 5–20 min; λ_{irr} = 520 nm; $P_{average}$ = 250 mW (delay: 205 μs); final pH = 6.5 ± 0.5; stirring. (C) UV-vis spectra in water of AuNPs-citrate, before KF addition (black line) and after 60 min in 0.3 M KF (red dashed line).

salts do not absorb in the visible spectral range, preventing their photoreaction under the conditions used in this study. All grafting experiments were conducted in water at pH 6.5 in presence of free citrate at room temperature (rt). This pH was chosen because AuNPs-citrate exhibit poor stability at pH < 6.5, while diazonium groups are unstable under basic conditions, readily forming diazoate groups that subsequently decompose into their corresponding radical species.[39,40] The following experimental parameters were optimized to enhance the grafting efficiency of the tetra-diazonium salt: irradiation time (τ_{irr}), laser output power (P), as well as the concentration of free citrate, AuNPs-citrate, and $X_4(PEG)_4(N_2^+)_4$. After each grafting experiment, the resulting functionalized particles (AuNPs–$X_4(PEG)_4$) were purified through four centrifugation cycles in water and stored at room temperature. The density of the organic ligand shell surrounding the AuNPs was evaluated using a simple and reliable stability test based on potassium fluoride treatment.[41] This assay monitors particle aggregation *via* UV-vis spectroscopy one hour after the addition of 0.3 M KF. Significant aggregation indicates a low ligand density, whereas the absence of aggregation suggests a densely grafted ligand shell. The extent of aggregation was quantified using the absorbance ratio $A(\lambda_{max})/A(700\ nm)$, which decreases as particles aggregate. This fluoride-based stability assay provided valuable insights into the key parameters required for efficient photo-assisted functionalization of AuNPs with calix[4]arenes. As a control experiment, functionalization of AuNPs-citrate by $X_4(PEG)_4(N_2^+)_4$ was first evaluated at pH 6.5 without any laser irradiation. Irreversible aggregation of the resulting nanoparticles occurred during the cleaning cycle, indicating poor surface coverage (Fig. S1). As shown in Fig. 1B, the resistance against fluoride of AuNPs–$X_4(PEG)_4$ increased with irradiation time, reaching a plateau after 15 minutes. In strong contrast to AuNPs-citrate, the UV-vis spectrum of AuNPs–$X_4(PEG)_4$ obtained after 20 min of irradiation showed no aggregation in the presence of fluoride (Fig. 1B *vs.* C). Only a slight decrease in absorbance was observed (Fig. 1B), likely due to weak adsorption of the PEG chains from the grafted calixarenes onto the cuvette walls.[41] Unlike classical ligand-exchange processes (Fig. S2), the functionalization efficiency was unaffected by the citrate concentration (from 0.05 mM to 1.2 mM).[42,43] Given the high optical absorption of AuNPs, the initial concentration of AuNPs-citrate proved to be a crucial parameter. Efficient grafting was only achieved at concentrations below 6 nM, corresponding to an absorbance of approximately 3 for 17 nm AuNPs (Fig. S3). At higher concentrations, grafting efficiency decreased, likely caused by the excessive light absorption of AuNP suspension. Interestingly, the amount of $X_4(PEG)_4(N_2^+)_4$ could be reduced to 40 000 eq. per NP without any changes in the stability of the NPs (Fig. S4), requiring substantially fewer reagents than the 100 000 equivalents typically required for classical chemical reduction with $NaBH_4$.[21] Finally, the laser output was found to be a crucial factor, with optimal grafting achieved at the maximum power, *i.e.* P = 250 mW. Lower power settings resulted in poor functionalization efficiency (Fig. S5).

A progressive decrease in absorbance was observed during the irradiation experiments. To investigate this effect, real-time UV-vis spectroscopy was used to monitor the grafting of $X_4(PEG)_4(N_2^+)_4$ onto AuNPs-citrate under 520 nm laser irradiation at different time points (Fig. 2A). A decline in absorbance, accompanied by a hypsochromic shift (from 523 to 516 nm) suggested a NP size reduction. Prolonged irradiation (>20 min) resulted in extensive size reduction, preventing most AuNPs from being recovered by centrifugation. Such a modification of AuNPs upon laser irradiation has been previously reported[44] and has been attributed to complex multistep fragmentation pathways, accompanied by solution-mediated etching and growth processes.[45,46] To mitigate this effect, different irradiation wavelengths (λ_{irr} = 450, 480, 518, 600, and 710 nm) were tested to reduce light absorption by shifting excitation away from the LSPR λ_{max} (Fig. 2B). A clear correlation was observed between the irradiation wavelength, and the extent of the absorbance loss, as evidenced by naked eye inspection of the resulting suspensions (Fig. 2C). Samples irradiated at 710 and 600 nm were subjected to a KF test to determine whether irradiation at these wavelengths still enabled the reductive grafting of the calix[4]arenes onto the particle surfaces. Irradiation at 710 nm resulted in minimal absorbance decrease (Fig. 2D) but produced poorly functionalized AuNPs (Fig. S6). The best balance was achieved at 600 nm, which significantly reduced absorbance loss compared to irradiation at LSPR λ_{max} (Fig. 2D) while yielding AuNPs–$X_4(PEG)_4$ with excellent robustness (Fig. 2E). TEM images of AuNPs–$X_4(PEG)_4$ functionalized under irradiation at these two wavelengths were recorded (Fig. 2F). Compared to the initial size of AuNPs-citrate (17.0 nm) (see Fig. S7 for TEM images and size distribution of AuNPs-citrate before irradiation), the images confirmed a more pronounced size reduction of the NPs obtained under irradiation at the LSPR λ_{max} (11.3 ± 1.5 nm) compared to 600 nm irradiation (13.8 ± 1.4 nm).

It is noteworthy that the presence of calix[4]arenes on the surface of the nanoparticles functionalized under irradiation at 600 nm was confirmed through infrared spectroscopy, with typical bands belonging to the calix[4]arene core and oEG groups at 1466 cm^{-1} (C_{Ar}–C_{Ar} ring stretch) and 1102 cm^{-1} (asymmetric COC stretching from the oEG chains), respectively (Fig. S8). Based on this first set of experiments, the optimized conditions were established as follows: [AuNPs-citrate] = 6 nM, $[X_4(PEG)_4(N_2^+)_4]$ = 40 000 eq./NP, [citrate] = 0.015–1.15 mM, λ_{irr} = 600 nm, τ_{irr} = 20 min, P = 250 mW, pH = 6.5, at rt (see Table S1 for the list of conditions that were evaluated during this optimization process). Compared to the conventional chemical reduction procedures we have previously reported,[47] these conditions offer significant advantages: the required amount of calixarene–tetradiazonium salt is reduced by half, and the grafting process is considerably faster (15–20 min *vs.* 16 h for

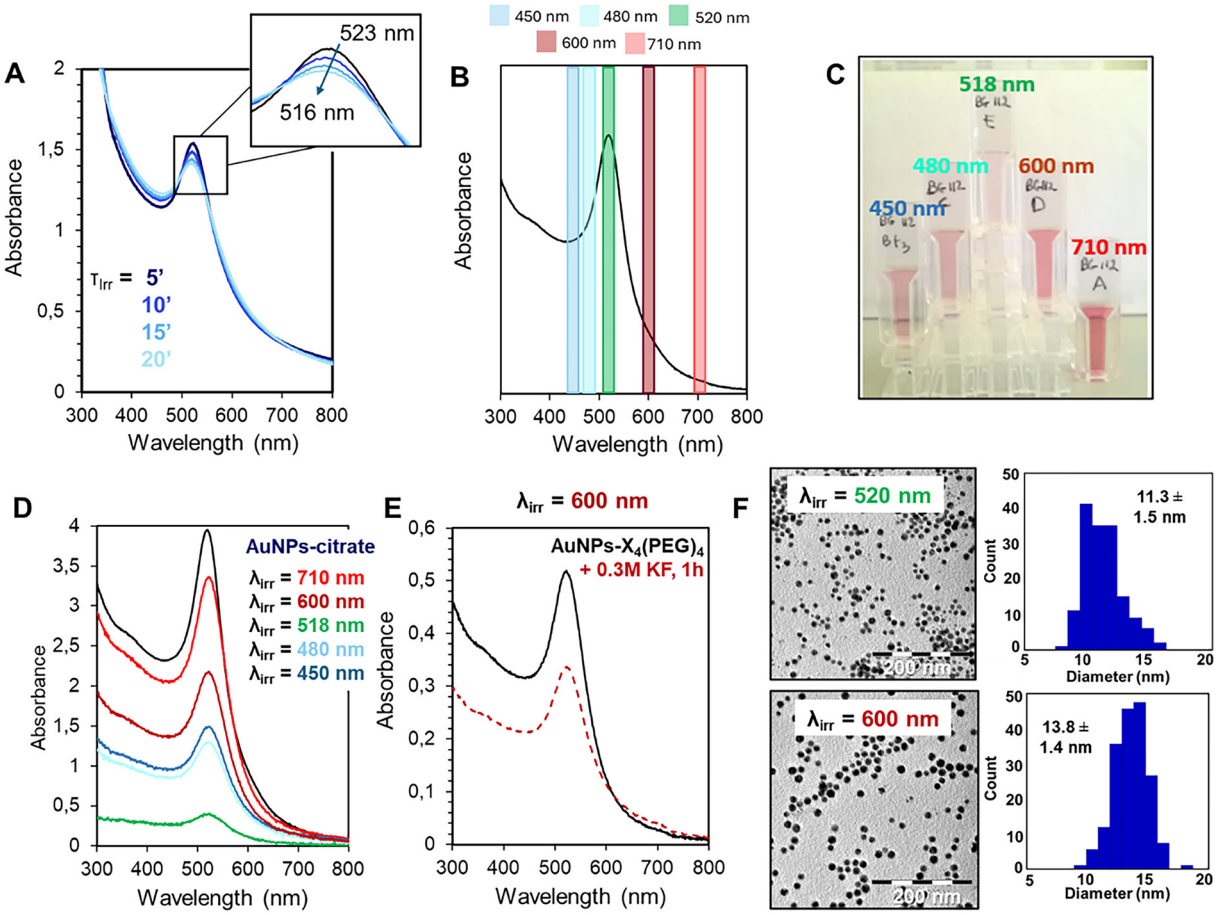

Fig. 2 (A) Spectrophotometric monitoring of the laser induced-grafting at 520 nm of $X_4(PEG)_4(N_2^+)_4$ onto AuNPs-citrate. UV-vis spectra were recorded with 5 min timelapse over 20 min of laser irradiation. (B) Position of the tested irradiation wavelengths on the absorbance spectrum of the AuNPs. (C) Picture of the various suspensions obtained at different irradiation wavelengths (the suspensions have been diluted 4 times). (D) UV-vis absorbance spectra of AuNPs-citrate before irradiation (black), AuNPs–$X_4(PEG)_4$ after 20 min under 450 nm (blue), 480 nm (cyan), 518 nm (green), 600 nm (dark red) or 710 nm (red) laser irradiation. (E) UV-vis absorption spectra of AuNPs–$X_4(PEG)_4$ obtained by laser induced-grafting at 600 nm, before KF addition (black line) and after 60 min in the presence of 0.3 M KF (red dashed line). (F) TEM image and size distribution (obtained by measuring the size of at least 150 particles) of AuNPs–$X_4(PEG)_4$ functionalized under irradiation at 520 nm (top) and at 600 nm (bottom). Experimental details: P = 250 mW, τ_{irr} = 20 minutes, stirring.

the chemical reduction method). It is worth mentioning that parameters such as temperature, pH and diazonium concentration influence the kinetics of the chemical functionalization. The conditions reported here were optimized to maximize the robustness of the resulting suspensions rather than the reaction rate.

Investigation of the grafting mechanism

Upon pulsed laser excitation, AuNPs can simultaneously generate hot electron and induce a temperature increase of their metallic core.[45,48] Both effects could contribute to the grafting of the tetra-diazonium salt. To gain insight into the grafting mechanism, AuNPs-citrate (6 nM) were irradiated at 520 nm and 600 nm (τ_{irr} = 10 min, P = 250 mW, pH = 6.5, at rt) in the presence of $K_3[Fe(CN)_6]$ (0.25 mM).† The photo-assisted generation of electrons was monitored using UV-vis absorption spectrophotometry by tracking Fe^{3+} reduction. Indeed, Fe^{3+} exhibits a characteristic absorbance band at 419 nm (with an extinction coefficient of 1050 M^{-1} cm^{-1}), while its reduced form, Fe^{2+}, does not absorb in the visible spectrum.[11] A significant decrease in absorbance at 419 nm was observed for both irradiation wavelengths (Fig. 3A and B). After 10 minutes of irradiation, 71% and 62% of Fe^{3+} was reduced to Fe^{2+} upon photoexcitation at 520 nm and 600 nm, respectively. In contrast, no Fe^{3+} reduction was detected under irradiation in the absence of AuNPs or without irradiation (Fig. S9 and S10), confirming that the reduction originated from electron generation by photoexcited AuNPs. Note that in the absence of Fe^{3+}, a decrease of the AuNPs absorbance was observed upon irradiation but no decrease was observed at 419 nm (Fig. S11). Additionally, post-irradiation temperature increases of 10 and 11 °C were measured for the suspensions irradiated at 520 nm and 600 nm, respectively. These values are

† A Fe^{3+} concentration of 0.25 mM was chosen, as it provides a tenfold excess of the electrons required to reduce a sufficient amount of diazonium salt to fully functionalize the surface of the AuNPs.

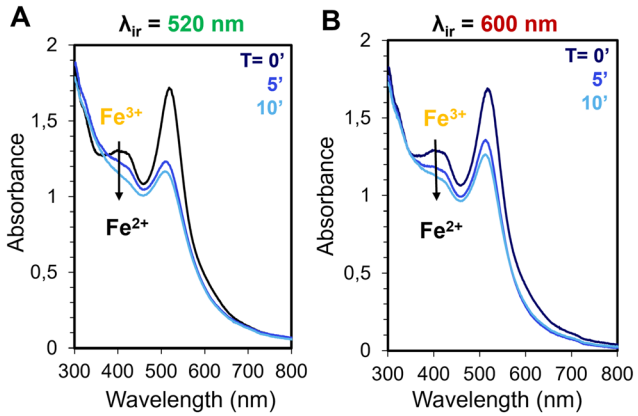

Fig. 3 Spectrophotometric monitoring of ferricyanide $[Fe(CN)_6]^{3-}$ (0.25 mM) reduction photocatalyzed by AuNPs-citrate (3 nM) under 250 mW laser excitation, at pH = 6.5 and continuous stirring. Time-series of UV-vis spectra are shown over 10 min of laser irradiation for two different irradiation wavelengths: (A) λ_{irr} = 520 nm (B) λ_{irr} = 600 nm.

consistent with previous reports.† All these data suggest that the laser-induced grafting of $X_4(PEG)_4(N_2^+)_4$ onto AuNPs-citrate could occur *via* hot electron generation and/or thermal decomposition.[49,50] Furthermore, the similar reduction efficiency and temperature rise observed for both irradiation wavelengths confirm that excitation at 600 nm is preferable, as it minimizes NP size reduction while maintaining effective functionalization.

Samples prepared either by irradiation at 600 nm and by chemical reduction were analysed by XPS and SERS to confirm the successful grafting of the tetra-diazonium salt. XPS analysis revealed marked differences in the surface chemistry of the AuNPs–$X_4(PEG)_4$ samples, depending on the grafting strategy. The XPS survey spectra show an increased carbon signal intensity relative to gold after laser-induced functionalization, compared to chemical reduction (Fig. 4). The pronounced attenuation of the Au signal observed following laser-induced grafting compared to chemical reduction indicates a more extensive organic coverage, suggesting a higher grafting efficiency. Interestingly, the high-resolution C 1s, O 1s, and N 1s spectra remain nearly identical for both grafting strategies, indicating that the $X_4(PEG)_4$ moieties are not chemically altered upon laser irradiation. In contrast, the Au 4f high-resolution spectra show a pronounced modification, characterized by a clear splitting of the 4f doublet after laser-induced grafting. Specifically, the Au 4f spectrum recorded after chemical grafting exhibits a single pair of

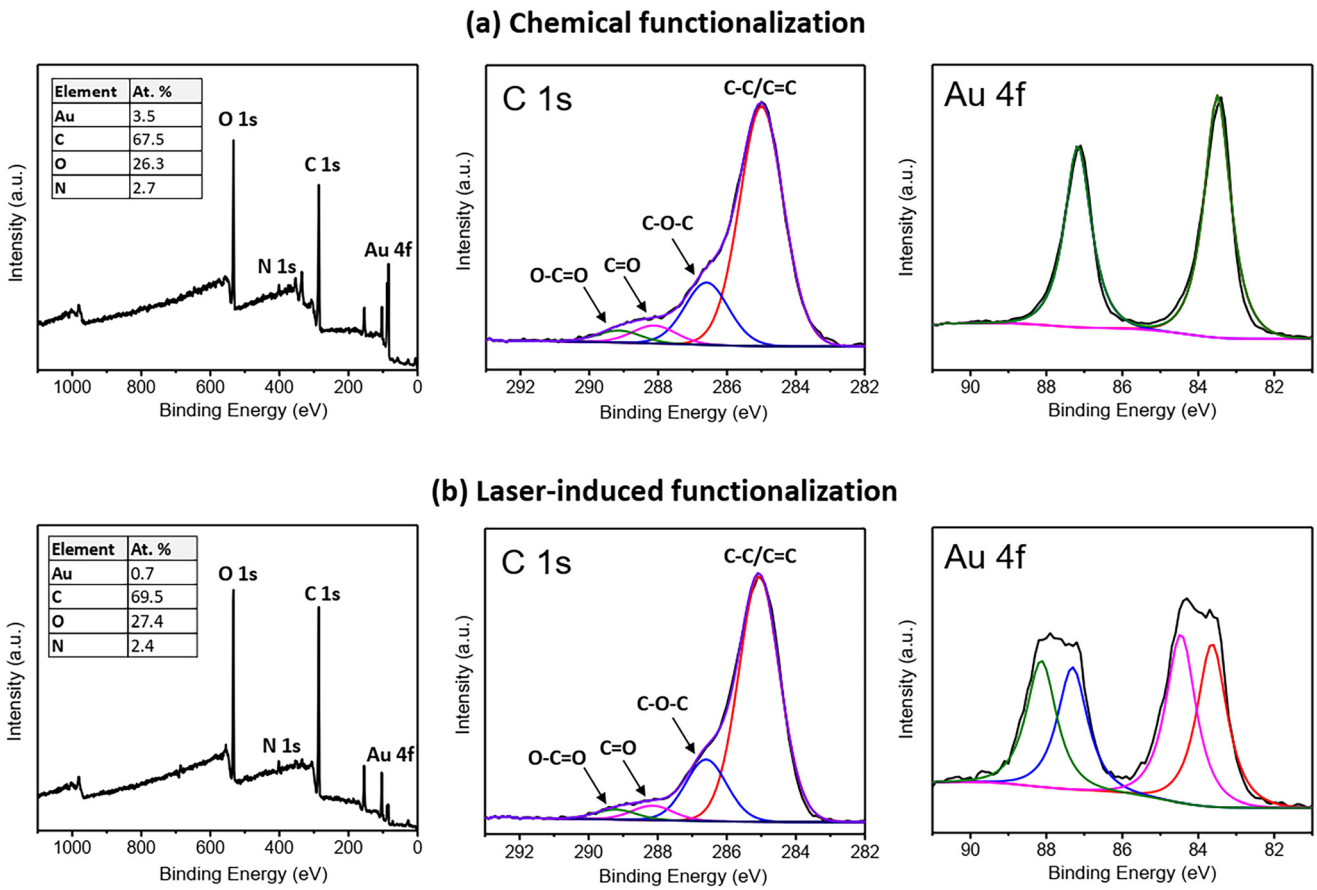

Fig. 4 XPS survey spectra and high-resolution C 1 s and Au 4f spectra of AuNPs–$X_4(PEG)_4$ prepared by (a) chemical or (b) laser-induced functionalization. Inset tables report the atomic compositions.

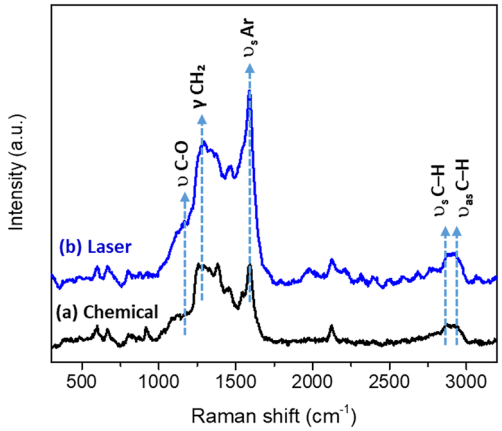

Fig. 5 Average SERS spectra of AuNPs–$X_4(PEG)_4$ prepared by (a) chemical or (b) laser-induced functionalization.

peaks at 83.5 eV and 87.2 eV (Fig. 4a), assigned to the Au $4f_{7/2}$ and Au $4f_{5/2}$ components of metallic gold (Au^0). After laser-induced grafting, an additional pair of peaks appears (Fig. 4b), attributable to oxidized gold species (Au^+) with binding energies of 84.5 eV and 88.1 eV. This partial oxidation could arise from photoinduced charge transfer processes between gold and $X_4(PEG)_4(N_2^+)_4$, promoted by the local electromagnetic fields generated during laser irradiation of the AuNPs.

The SERS spectra of the AuNPs–$X_4(PEG)_4$ samples confirmed the successful coating of the AuNPs with the calix[4]arene layer. Characteristic vibrational features from both the aryl rings (ν(C═C) at 1590 cm^{-1}) and the oligo(ethylene glycol) chains (symmetric and antisymmetric ν(C–H) at 2880 and 2940 cm^{-1}, CH_2 wagging at 1280 cm^{-1}, and ν(C–O) at 1150 cm^{-1}) were clearly observed (Fig. 5). Although the overall spectral profiles remained similar regardless of the grafting strategy, the averaged spectra recorded over the entire surface of the deposited drops revealed a higher overall intensity for the laser-induced grafting, suggesting a more efficient surface coverage, in agreement with the XPS results.

Extension to other diazonium salts

Finally, we explored whether the optimized laser-induced functionalization protocol could be extended to other diazonium salts. To this end, two additional systems were selected: a calix[4]arene tetra-diazonium salt bearing four carboxyl groups on the small rim ($X_4(COOH)_4(N_2^+)_4$) and a pegylated aryl diazonium salt (aryl(PEG)N_2^+) (Fig. 6A). Pulsed laser irradiation of 17 nm AuNPs-citrate in the presence of $X_4(COOH)_4(N_2^+)_4$ under the optimized conditions (*vide supra*) resulted in efficient functionalization. The presence of calix[4]arenes on the surface of the resulting AuNPs–$X_4(COOH)_4$ was confirmed through infrared spectroscopy, with characteristic peaks at 1604 cm^{-1} (CO_2 ν_{asym}) and 1459 cm^{-1} (C_{Ar}–C_{Ar} ring stretch) (Fig. S12). These particles exhibited a remarkable stability in the fluoride-based assay, indicating a dense organic shell on the AuNP surface (Fig. 6B). For comparison, a batch of AuNPs–$X_4(COOH)_4$ was also prepared using the classical procedure with $NaBH_4$ as reducing agent.[47] While both approaches yielded particles with similar fluoride stability (Fig. 6B *vs.* C), it is noteworthy that the laser-induced functionalization was significantly faster (20 min *vs.* 16 h) and required only half the amount of calixarene diazonium salt.

In contrast, functionalization with the aryl(PEG) diazonium salt led to particles with much lower stability in the fluoride assay, regardless of whether laser-induced or chemical grafting was used (Fig. S13). Nonetheless, slightly improved stability was observed for the nanoparticles produced *via* the laser-induced method. This reduced stability can be attributed to the nature of the aryl diazonium-derived coating, which is known to form loosely bound, cauliflower-like polymeric layers.[51] In comparison, calix[4]arene-based diazonium salts inherently prevent such uncontrolled polymerization due to their macrocyclic structure. Moreover, each grafted calix[4]arene is able to anchor to the nanoparticle surface through multiple covalent bonds, resulting in highly robust and densely packed organic layers.

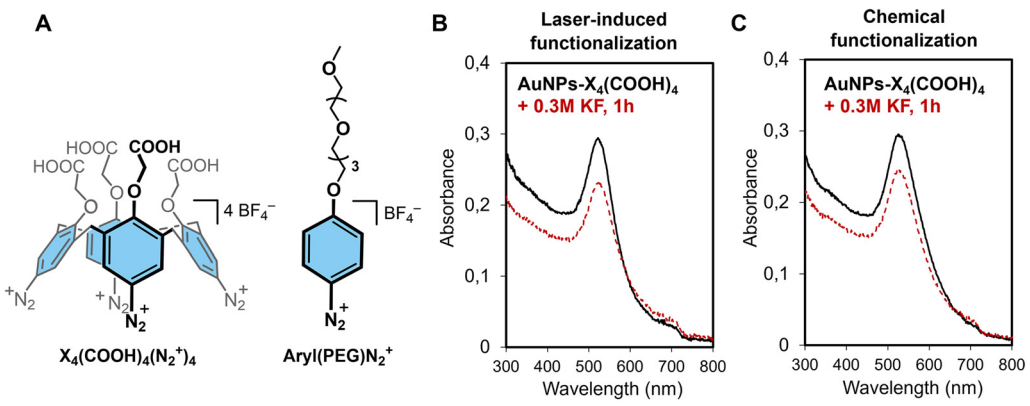

Fig. 6 (A) Structures of $X_4(COOH)_4(N_2^+)_4$ and aryl(PEG)N_2^+. UV-vis absorption spectra in water of AuNPs–$X_4(COOH)_4$ functionalized by the laser-induced procedure (B) or the reported chemical procedure (C), before KF addition (black) and after 60 min in 0.3 M KF (red dashed line).

Conclusion

We have developed a novel plasmon-mediated strategy for the rapid and efficient functionalization of colloidal gold nanoparticles using calix[4]arene-based tetra-diazonium salts under pulsed laser irradiation. By leveraging the localized surface plasmon resonance of AuNPs, our method enables reductive grafting without the need for chemical reducing agents or photocatalysts. While irradiation at the LSPR maximum (520 nm) induced severe nanoparticle fragmentation due to intense localized heating, shifting the irradiation wavelength to 600 nm significantly reduced particle size reduction while maintaining efficient surface functionalization. The optimized functionalization process was shown to be both time- (≤20 min) and resource-efficient, requiring significantly lower amounts of diazonium salt compared to conventional chemical methods. Mechanistic investigations confirmed that the grafting proceeds *via* a combination of hot electron generation and/or localized heating. Both SERS and XPS surveys confirmed the presence of a calix[4]arene layer on the particles, with a denser coating observed following laser-induced functionalization. The versatility of the method was demonstrated through its successful achievement on two structurally distinct calix[4]arene-based diazonium salts, with superior grafting performance relative to classical aryl diazonium salts. Overall, this plasmon-assisted approach appears as particularly promising for the robust and scalable surface modification of colloidal plasmonic nanoparticles, opening new avenues for applications in nanomedicine, sensing, and catalysis. Ongoing work aims to expand this strategy to other types of plasmonic nanomaterials.

Experimental section

Synthesis of aryl diazonium derivatives and gold nanoparticles

The synthesis of aryl(PEG) diazonium, $X_4(PEG)_4(N_2^+)_4$ and $X_4(COOH)_4(N_2^+)_4$ were achieved according to previously reported procedures.[20,38] AuNPs–citrate were synthesized by the reduction of $KAuCl_4$ with citrate using a modified Turkevich method and dialyzed against a 1 mM solution of sodium citrate.[52] TEM characterization showed mainly spherical AuNPs with an average core diameter of 17.0 nm. Aqueous solutions were prepared either in Millipore or in Lichrosolv water.

Fe^{3+} reduction experiments

In a 4 mL PMMA-cell, 1000 μL of citrate gold nanoparticles (2–3 nM with 0.5 mM citrate) and 24 μL of $K_3[Fe(CN)_6]$ (10 mM) were added successively. Then, the colloidal suspension was irradiated with the laser (delay = 205 μs) at the appropriate wavelength (520 nm or 600 nm depending on the experiment) for 0, 5 and 10 minutes under stirring. UV-vis absorption spectra of the suspension were recorded for each irradiation time.

Optimized laser-induced grafting procedure

AuNPs-citrate (17 nm, 600 μL, 10 nM, 7 pmol) were placed in 4 mL PMMA cell with a 4 mm stir bar. 400 μL of H_2O Lichrosolv and 5 μL of NaOH 0.5 M were added. Then, a solution of calix[4]arene (60 μL, 5 mM, 0.3 μmol) was added over 1 min (pH value of 6.5 ± 0.5 after the addition). The cell was irradiated for 20 minutes upon pulsed laser (delay = 205 μs, 250 mW) at 600 nm, after which the stir bars were removed, and water (500 μL) was added. The samples were transferred into a 1.5 mL Protein LoBind Eppendorf and centrifuged for 20 min at 18 000*g*, after which the supernatant was removed and the AuNPs were resuspended in H_2O. This process was repeated three times with Lichrosolv water (1.5 mL). At the end of the final cycle, the AuNPs were suspended in water (600 μL) and stored at room temperature for further characterization.

Control experiment: grafting procedure without any laser irradiation

AuNPs-citrate (17 nm, 600 μL, 10 nM, 7 pmol) were placed in 4 mL PMMA cell with a 4 mm stir bar, and 400 μL of H_2O Lichrosolv was added and 5 μL of NaOH 0.5 M. Then a calixarene solution (60 μL, 5 mM, 0.3 μmol) was added over 1 min. After the addition, the pH should reach a value: 6.5 ± 0.5. The mixture was stirred for 20 minutes, after which the stir bars were removed, and water (500 μL) was added. The samples were transferred into 1.5 mL Protein LoBind Eppendorf and centrifuged for 20 min at 18 000*g*, after which the supernatant was removed and the AuNPs were resuspended in H_2O. This process was repeated three times with Lichrosolv water (1.5 mL). At the end of the final cycle, the AuNPs were suspended in water (600 μL) and stored at room temperature for further characterization.

Chemical grafting procedure

AuNPs-citrate (17 nm, 600 μL, 10 nM, 7 pmol) were placed in 4 mL PMMA cell with a 4 mm stir bar. 400 μL of H_2O Lichrosolv, 5 μL of NaOH 0.5 M and 10 μL of $NaBH_4$ 0.1 M were added successively. Then, a solution of calix[4]arene (60 μL, 5 mM, 0.3 μmol) was added over 1 min (pH value of 6.5 ± 0.5 after the addition). The mixture was stirred for 16 h, after which the stir bars were removed, and water (500 μL) was added. The samples were transferred into 1.5 mL Protein LoBind Eppendorf and centrifuged for 20 min at 18 000*g*, after which the supernatant was removed and the AuNPs were resuspended in H_2O. This process was repeated three times with Lichrosolv water (1.5 mL). At the end of the final cycle, the AuNPs were suspended in water (600 μL) and stored at room temperature for further characterization.

Stability against fluoride test[41]

A first UV-vis absorption spectrum of AuNPs was recorded after the functionalization with a diazonium salt (cleaning step included). Then, the resulting functionalized AuNPs

were exposed to 0.3 M of potassium fluoride (KF) for 60 minutes. After this period of exposure, a second UV-vis spectrum was recorded. By comparing the ratio of the absorbance at 680 nm and 520 nm before and after the KF addition, it was possible to evaluate the level of nanoparticles functionalization. Densely functionalized nanoparticles present no or few variations after the KF addition while partly functionalized nanoparticles present variations proportional to their level of functionalization.

Characterization measurement

Electronic UV-vis absorption spectra were recorded with a Shimadzu UV3600 spectrophotometer in disposable semi-micro cuvettes (PMMA). AuNPs were diluted by a 5 factor in 1 mL aqueous solution, except if specified. ATR-FTIR spectra were recorded at 20° Cona Bruker Equinox 55 spectrophotometer equipped with a liquid-nitrogen-cooled mercury–cadmium–telluride (MCT) detector. The gold nanoparticles were centrifugated and 2 μL of AuNPs "bottom" was deposited on a germanium internal reflection element (triangular prism of 6.8 × 45 mm^2 with an internal angle of incidence of 45°, ACM France) and the water was removed with a flow of nitrogen gas. Opus software (4.2.37) was used to record 128 scans with a resolution of 2 cm^{-1} under a continuous flow of nitrogen gas over the sample. Data were processed and analysed using the kinetics software in MatLab 7.1 (Mathworks Inc., Natick, MA) by the subtraction of water vapour, baseline correction, apodization at 4 cm^{-1}, and flattening of the CO_2 signal. Finally, the spectra were normalized at 1459 cm^{-1} (aromatic ring stretching band from the calixarenes) to compensate for variations in the number of AuNPs present on the spot at the Ge crystal where the measurement was performed. Images of the AuNPs were obtained with a Philips CM20-UltraTWIN Transmission Electron Microscope (TEM) equipped with a lanthanum hexaboride (LaB6) crystal at a 200 kV accelerating voltage. The average size and standard deviation were determined by measuring the size of more than 150 AuNPs. The pulsed laser is an Nd:YAG (Q-switched, Continuum Inc.) corresponding to neodymium doped yttrium aluminium garnet. This crystal is excited with a flashlight and produced radiation at 1064 nm. This radiation goes through a frequency multiplicator, which produces 2 radiations: at 532 nm and at 355 nm. The radiation at 355 nm can pass through an oscillator (OPO, continuum Inc.) that allows to produce laser irradiation wavelength in the range of 410–710 nm.

XPS analyses were carried out using an Omicron Argus X-ray photoelectron spectrometer, equipped with a monochromated Al Kα radiation source ($h\nu$ = 1486.6 eV) and a 280 W electron beam power. Photoelectron emission from the samples was analysed at a collection angle of 45° under ultra-high vacuum conditions ($\leq 10^{-9}$ mBar). Survey scans were recorded with a pass energy of 100 eV, while core-level spectra were acquired using a pass energy of 20 eV. Binding energies were referenced to the C 1s peak at 284.8 eV, and peak intensities were corrected using Scofield factors. Peak areas were determined after subtraction of a U 2 Tougaard background. Spectra were fitted using Casa XPS software (Casa Software Ltd, U.K.), applying a Gaussian/Lorentzian ratio of 70/30 for deconvolution.

SERS measurements were recorded using a Horiba XploRA PLUS Raman microscope. All spectra were acquired on dried drops of the samples deposited on aluminum foil, using a 638 nm laser, with an exposure time of 10 s and an accumulation of 10 spectra.

Conflicts of interest

There are no conflicts of interest to declare.

Data availability

The data supporting this article have been included as part of the supplementary information (SI). Supplementary information: stability tests of the different AuNP batches, optimization of the functionalization conditions of the AuNPs with $X_4(PEG)_4$ under laser irradiation and control experiments involving $[Fe(CN)_6]^{3-}$ and aryldiazoniums are available in the SI. See DOI: https://doi.org/10.1039/d5lf00197h.

Acknowledgements

Antoine Miche is gratefully acknowledged for his help in conducting XPS experiments. The spectrometer was funded by Sorbonne Université, CNRS and Région Ile de France, and is part of FCMat, The Federation of Chemistry and Materials of Paris-Center. Ludovic Troian-Gauthier (UCLouvain, Belgium) is gratefully acknowledged for providing access to a laser equipment that has allowed to produce the additional samples for the XPS and SERS analysis. This research was supported by the Fonds pour la formation à la Recherche dans l'Industrie et dans l'Agriculture (FRIA-FRS) and the Fonds David et Alice Van Buuren (PhD grant to B. G.) and by the "Actions de Recherches Concertées" (grant "New very high density protein microarrays for ligand binding detection by FTIR imaging") of the Fédération Wallonie-Bruxelles and the ULB (PhD grant to M. R.). J. T. was a teaching assistant at the ULB.

References

1 K. L. Kelly, E. Coronado, L. L. Zhao and G. C. Schatz, The Optical Properties of Metal Nanoparticles: The Influence of Size, Shape, and Dielectric Environment, *J. Phys. Chem. B*, 2003, **107**(3), 668–677, DOI: 10.1021/jp026731y.

2 M. Broadbent, S. J. Chadwick, M. Brust and M. Volk, Gold Nanoparticles for Photothermal and Photodynamic Therapy, *ACS Omega*, 2024, **9**(44), 44846–44859, DOI: 10.1021/acsomega.4c08797.

3 M. Gul, M. Kashif, S. Muhammad, S. Azizi and H. Sun, Various Methods of Synthesis and Applications of Gold-Based Nanomaterials: A Detailed Review, *Cryst. Growth Des.*, 2025, acs.cgd.4c01687, DOI: 10.1021/acs.cgd.4c01687.

4 Y.-S. Borghei, S. Hosseinkhani and M. R. Ganjali, "Plasmonic Nanomaterials": An Emerging Avenue in Biomedical and Biomedical Engineering Opportunities, *J. Adv. Res.*, 2022, **39**, 61–71, DOI: 10.1016/j.jare.2021.11.006.
5 R. García-Álvarez, L. Chen, A. Nedilko, A. Sánchez-Iglesias, A. Rix, W. Lederle, V. Pathak, T. Lammers, G. Von Plessen, K. Kostarelos, L. M. Liz-Marzán, A. J. C. Kuehne and D. N. Chigrin, Optimizing the Geometry of Photoacoustically Active Gold Nanoparticles for Biomedical Imaging, *ACS Photonics*, 2020, **7**(3), 646–652, DOI: 10.1021/acsphotonics.9b01418.
6 J. Zhao, S. C. Nguyen, R. Ye, B. Ye, H. Weller, G. A. Somorjai, A. P. Alivisatos and F. D. Toste, A Comparison of Photocatalytic Activities of Gold Nanoparticles Following Plasmonic and Interband Excitation and a Strategy for Harnessing Interband Hot Carriers for Solution Phase Photocatalysis, *ACS Cent. Sci.*, 2017, **3**(5), 482–488, DOI: 10.1021/acscentsci.7b00122.
7 J. Lee, P. B. Joshi, A. J. Wilson and Y. Kim, Plasmon-Driven Near-Field Photopolymerization in a Gold Nanoparticle Colloid, *J. Phys. Chem. C*, 2023, **127**(17), 8096–8103, DOI: 10.1021/acs.jpcc.3c01461.
8 Q. Lenne, M. Retout, B. Gosselin, G. Bruylants, I. Jabin, J. Hamon, C. Lagrost and Y. R. Leroux, Highly Stable Silver Nanohybrid Electrocatalysts for the Oxygen Reduction Reaction, *Chem. Commun.*, 2022, **58**(20), 3334–3337, DOI: 10.1039/D2CC00637E.
9 L. Zhou, Q. Huang and Y. Xia, Plasmon-Induced Hot Electrons in Nanostructured Materials: Generation, Collection, and Application to Photochemistry, *Chem. Rev.*, 2024, **124**(14), 8597–8619, DOI: 10.1021/acs.chemrev.4c00165.
10 S. Yu, A. J. Wilson, J. Heo and P. K. Jain, Plasmonic Control of Multi-Electron Transfer and C–C Coupling in Visible-Light-Driven CO_2 Reduction on Au Nanoparticles, *Nano Lett.*, 2018, **18**(4), 2189–2194, DOI: 10.1021/acs.nanolett.7b05410.
11 Y. Kim, J. G. Smith and P. K. Jain, Harvesting Multiple Electron–Hole Pairs Generated through Plasmonic Excitation of Au Nanoparticles, *Nat. Chem.*, 2018, **10**(7), 763–769, DOI: 10.1038/s41557-018-0054-3.
12 C. Zhang, J. Qi, Y. Li, Q. Han, W. Gao, Y. Wang and J. Dong, Surface-Plasmon-Assisted Growth, Reshaping and Transformation of Nanomaterials, *Nanomaterials*, 2022, **12**(8), 1329, DOI: 10.3390/nano12081329.
13 G. González-Rubio, P. Díaz-Núñez, A. Rivera, A. Prada, G. Tardajos, J. González-Izquierdo, L. Bañares, P. Llombart, L. G. Macdowell, M. Alcolea Palafox, L. M. Liz-Marzán, O. Peña-Rodríguez and A. Guerrero-Martínez, Femtosecond Laser Reshaping Yields Gold Nanorods with Ultranarrow Surface Plasmon Resonances, *Science*, 2017, **358**(6363), 640–644, DOI: 10.1126/science.aan8478.
14 J. Fan, Y. Cheng and M. Sun, Functionalized Gold Nanoparticles: Synthesis, Properties and Biomedical Applications, *Chem. Rec.*, 2020, **20**(12), 1474–1504, DOI: 10.1002/tcr.202000087.
15 A. Heuer-Jungemann, N. Feliu, I. Bakaimi, M. Hamaly, A. Alkilany, I. Chakraborty, A. Masood, M. F. Casula, A. Kostopoulou, E. Oh, K. Susumu, M. H. Stewart, I. L. Medintz, E. Stratakis, W. J. Parak and A. G. Kanaras, The Role of Ligands in the Chemical Synthesis and Applications of Inorganic Nanoparticles, *Chem. Rev.*, 2019, **119**(8), 4819–4880, DOI: 10.1021/acs.chemrev.8b00733.
16 S. M. Ansar, F. S. Mohammed, G. Von White, M. Budi, K. C. Powell, O. T. Mefford and C. L. Kitchens, Effect of Postsynthesis Purifications on Gold and Silver Nanoparticle Ligand Coverage, *J. Phys. Chem. C*, 2016, **120**(12), 6842–6850, DOI: 10.1021/acs.jpcc.5b12423.
17 S. A. Orefuwa, M. Ravanbakhsh, S. N. Neal, J. B. King and A. A. Mohamed, Robust Organometallic Gold Nanoparticles, *Organometallics*, 2014, **33**(2), 439–442, DOI: 10.1021/om400927g.
18 D. Hetemi, V. Noël and J. Pinson, Grafting of Diazonium Salts on Surfaces: Application to Biosensors, *Biosensors*, 2020, **10**(1), 4, DOI: 10.3390/bios10010004.
19 L. Laurentius, S. R. Stoyanov, S. Gusarov, A. Kovalenko, R. Du, G. P. Lopinski and M. T. McDermott, Diazonium-Derived Aryl Films on Gold Nanoparticles: Evidence for a Carbon–Gold Covalent Bond, *ACS Nano*, 2011, **5**(5), 4219–4227, DOI: 10.1021/nn201110r.
20 A. Mattiuzzi, I. Jabin, C. Mangeney, C. Roux, O. Reinaud, L. Santos, J.-F. Bergamini, P. Hapiot and C. Lagrost, Electrografting of Calix[4]Arenediazonium Salts to Form Versatile Robust Platforms for Spatially Controlled Surface Functionalization, *Nat. Commun.*, 2012, **3**(1), 1130, DOI: 10.1038/ncomms2121.
21 L. Troian-Gautier, A. Mattiuzzi, O. Reinaud, C. Lagrost and I. Jabin, Use of Calixarenes Bearing Diazonium Groups for the Development of Robust Monolayers with Unique Tailored Properties, *Org. Biomol. Chem.*, 2020, **18**(19), 3624–3637, DOI: 10.1039/D0OB00070A.
22 M. Retout, B. Gosselin, A. Adrović, P. Blond, I. Jabin and G. Bruylants, Ultra-Stable Silver Nanoplates: Efficient and Versatile Colorimetric Reporters for Dipstick Assays, *Nanoscale*, 2023, **15**(28), 11981–11989, DOI: 10.1039/D3NR02378H.
23 H. Valkenier, V. Malytskyi, P. Blond, M. Retout, A. Mattiuzzi, J. Goole, V. Raussens, I. Jabin and G. Bruylants, Controlled Functionalization of Gold Nanoparticles with Mixtures of Calix[4]Arenes Revealed by Infrared Spectroscopy, *Langmuir*, 2017, **33**(33), 8253–8259, DOI: 10.1021/acs.langmuir.7b02140.
24 M. Retout, B. Cornelio, G. Bruylants and I. Jabin, Bifunctional Calix[4]Arene-Coated Gold Nanoparticles for Orthogonal Conjugation, *Langmuir*, 2022, **38**(30), 9301–9309, DOI: 10.1021/acs.langmuir.2c01122.
25 B. Gosselin, G. Bruylants and I. Jabin, Tailored Ultrastable Core–Shell Au@Ag Nanoparticles for Enhanced Colorimetric Detection in Lateral Flow Assays, *ACS Appl. Nano Mater.*, 2024, acsanm.3c06070, DOI: 10.1021/acsanm.3c06070.
26 C. Darviot, B. Gosselin, F. Martin, S. Patskovsky, I. Jabin, G. Bruylants, D. Trudel and M. Meunier, Multiplexed Immunolabelling of Cancer Using Bioconjugated Plasmonic Gold–Silver Alloy Nanoparticles, *Nanoscale Adv.*, 2024, **6**(17), 4385–4393, DOI: 10.1039/D4NA00052H.
27 V. Lepeintre, F. Camerel, C. Lagrost, M. Retout, G. Bruylants and I. Jabin, Calixarene-Coated Gold Nanorods as Robust

Photothermal Agents, *Nanoscale*, 2024, **16**(42), 19692–19703, DOI: 10.1039/D4NR02296C.

28 C. Moya, N. Brion, L. Troian-Gautier, I. Jabin and G. Bruylants, Robust Calix[4]Arene-Polyethyleneimine Coated Iron Oxide Nanoparticles for Enhanced Recovery of Gold and Platinum Chloride Complexes, *Environ. Sci.: Nano*, 2025, **12**(1), 777–790, DOI: 10.1039/D4EN00408F.

29 T. T. A. Nguyen, R. Dutour, L. Conrard, M. Vermeersch, M. Mirgaux, D. Perez-Morga, N. Baeyens, G. Bruylants and I. Demeestere, Effect of Surface Modification of Gold Nanoparticles Loaded with Small Nucleic Acid Sequences on Cytotoxicity and Uptake: A Comparative Study In Vitro, *ACS Appl. Bio Mater.*, 2025, **8**(4), 3040–3051, DOI: 10.1021/acsabm.4c01861.

30 A. Olshtrem, O. Guselnikova, P. Postnikov, A. Trelin, M. Yusubov, Y. Kalachyova, L. Lapcak, M. Cieslar, P. Ulbrich, V. Svorcik and O. Lyutakov, Plasmon-Assisted Grafting of Anisotropic Nanoparticles – Spatially Selective Surface Modification and the Creation of Amphiphilic SERS Nanoprobes, *Nanoscale*, 2020, **12**(27), 14581–14588, DOI: 10.1039/D0NR02934C.

31 A. Olshtrem, E. Miliutina, P. Sajdl, V. Burtsev, M. Erzina, M. Vondracek, P. Postnikov, J. Lancok, V. Svorcik, S. Chertopalov and O. Lyutakov, Plasmon-Assisted Spatially Selective Grafting of Ti3C2TX Flakes for Prevention of MXene Oxidation and Stability Increase, *Chem. Eng. J.*, 2023, **476**, 146399, DOI: 10.1016/j.cej.2023.146399.

32 M. Busson, A. Berisha, C. Combellas, F. Kanoufi and J. Pinson, Photochemical Grafting of Diazonium Salts on Metals, *Chem. Commun.*, 2011, **47**(47), 12631, DOI: 10.1039/c1cc16241a.

33 M. Busson, A. Berisha, C. Combellas, F. Kanoufi and J. Pinson, Photochemical Grafting of Diazonium Salts on Metals, *Chem. Commun.*, 2011, **47**(47), 12631, DOI: 10.1039/c1cc16241a.

34 M. Nguyen, A. Lamouri, C. Salameh, G. Lévi, J. Grand, L. Boubekeur-Lecaque, C. Mangeney and N. Félidj, Plasmon-Mediated Chemical Surface Functionalization at the Nanoscale, *Nanoscale*, 2016, **8**(16), 8633–8640, DOI: 10.1039/C6NR00744A.

35 I. Kherbouche, Y. Luo, N. Félidj and C. Mangeney, Plasmon-Mediated Surface Functionalization: New Horizons for the Control of Surface Chemistry on the Nanoscale, *Chem. Mater.*, 2020, **32**(13), 5442–5454, DOI: 10.1021/acs.chemmater.0c00921.

36 V.-Q. Nguyen, Y. Ai, P. Martin and J.-C. Lacroix, Plasmon-Induced Nanolocalized Reduction of Diazonium Salts, *ACS Omega*, 2017, **2**(5), 1947–1955, DOI: 10.1021/acsomega.7b00394.

37 J. Pinson and F. Podvorica, Attachment of Organic Layers to Conductive or Semiconductive Surfaces by Reduction of Diazonium Salts, *Chem. Soc. Rev.*, 2005, **34**(5), 429, DOI: 10.1039/b406228k.

38 P. Blond, A. Mattiuzzi, H. Valkenier, L. Troian-Gautier, J.-F. Bergamini, T. Doneux, E. Goormaghtigh, V. Raussens and I. Jabin, Grafting of Oligo(Ethylene Glycol)-Functionalized Calix[4]Arene-Tetradiazonium Salts for Antifouling Germanium and Gold Surfaces, *Langmuir*, 2018, **34**(21), 6021–6027, DOI: 10.1021/acs.langmuir.8b00464.

39 L. Troian-Gautier, D. E. Martínez-Tong, J. Hubert, F. Reniers, M. Sferrazza, A. Mattiuzzi, C. Lagrost and I. Jabin, Controlled Modification of Polymer Surfaces through Grafting of Calix[4]Arene-Tetradiazoate Salts, *J. Phys. Chem. C*, 2016, **120**(40), 22936–22945, DOI: 10.1021/acs.jpcc.6b06143.

40 F. I. Podvorica, F. Kanoufi, J. Pinson and C. Combellas, Spontaneous Grafting of Diazoates on Metals, *Electrochim. Acta*, 2009, **54**(8), 2164–2170, DOI: 10.1016/j.electacta.2008.10.017.

41 M. Retout, B. Gosselin, J. V. Jokerst, I. Jabin and G. Bruylants, A Fluoride-Induced Aggregation Test to Quickly Assess the Efficiency of Ligand Exchange Procedures from Citrate Capped AuNPs, *Colloids Surf., A*, 2023, **660**, 130801, DOI: 10.1016/j.colsurfa.2022.130801.

42 J.-W. Park and J. S. Shumaker-Parry, Structural Study of Citrate Layers on Gold Nanoparticles: Role of Intermolecular Interactions in Stabilizing Nanoparticles, *J. Am. Chem. Soc.*, 2014, **136**(5), 1907–1921, DOI: 10.1021/ja4097384.

43 J.-W. Park and J. S. Shumaker-Parry, Strong Resistance of Citrate Anions on Metal Nanoparticles to Desorption under Thiol Functionalization, *ACS Nano*, 2015, **9**(2), 1665–1682, DOI: 10.1021/nn506379m.

44 X. Liu, M. Atwater, J. Wang and Q. Huo, Extinction Coefficient of Gold Nanoparticles with Different Sizes and Different Capping Ligands, *Colloids Surf., B*, 2007, **58**(1), 3–7, DOI: 10.1016/j.colsurfb.2006.08.005.

45 Z. Peng, T. Walther and K. Kleinermanns, Influence of Intense Pulsed Laser Irradiation on Optical and Morphological Properties of Gold Nanoparticle Aggregates Produced by Surface Acid–Base Reactions, *Langmuir*, 2005, **21**(10), 4249–4253, DOI: 10.1021/la047272q.

46 G. Bongiovanni, P. K. Olshin, C. Yan, J. M. Voss, M. Drabbels and U. J. Lorenz, The Fragmentation Mechanism of Gold Nanoparticles in Water under Femtosecond Laser Irradiation, *Nanoscale Adv.*, 2021, **3**(18), 5277–5283, DOI: 10.1039/D1NA00406A.

47 L. Troian-Gautier, H. Valkenier, A. Mattiuzzi, I. Jabin, N. V. Den Brande, B. V. Mele, J. Hubert, F. Reniers, G. Bruylants, C. Lagrost and Y. Leroux, Extremely Robust and Post-Functionalizable Gold Nanoparticles Coated with Calix[4]Arenes via Metal–Carbon Bonds, *Chem. Commun.*, 2016, **52**(69), 10493–10496, DOI: 10.1039/C6CC04534K.

48 S. K. Ghosh and T. Pal, Interparticle Coupling Effect on the Surface Plasmon Resonance of Gold Nanoparticles: From Theory to Applications, *Chem. Rev.*, 2007, **107**(11), 4797–4862, DOI: 10.1021/cr0680282.

49 P. S. J. Canning, K. McCrudden, H. Maskill and B. Sexton, Rates and Mechanisms of the Thermal Solvolytic Decomposition of Arenediazonium Ions, *J. Chem. Soc., Perkin Trans. 2*, 1999(12), 2735–2740, DOI: 10.1039/a905567c.

50 J. Pinson, Attachment of Organic Layers to Materials Surfaces by Reduction of Diazonium Salts, in *Aryl Diazonium Salts*, ed. Chehimi, M. M., Wiley, 2012, pp. 1–35, DOI: 10.1002/9783527650446.ch1.
51 S. Mahouche-Chergui, S. Gam-Derouich, C. Mangeney and M. M. Chehimi, Aryl Diazonium Salts: A New Class of Coupling Agents for Bonding Polymers, Biomacromolecules and Nanoparticles to Surfaces, *Chem. Soc. Rev.*, 2011, **40**(7), 4143, DOI: 10.1039/c0cs00179a.
52 M. Doyen, K. Bartik and G. Bruylants, UV–Vis and NMR Study of the Formation of Gold Nanoparticles by Citrate Reduction: Observation of Gold–Citrate Aggregates, *J. Colloid Interface Sci.*, 2013, **399**, 1–5, DOI: 10.1016/j.jcis.2013.02.040.